Article

The Spectral Elucidation versus the X-ray Structure of the Critical Precursor Complex in Bimolecular Electron Transfers: Application of Experimental/Theoretical Solvent Probes to Ion-Radical (Redox) Dyads

Sergiy V. Rosokha, Marshall D. Newton, Almaz S. Jalilov, and Jay K. Kochi

More About This Article

Additional resources and features associated with this article are available within the HTML version:

- Supporting Information
- Links to the 2 articles that cite this article, as of the time of this article download
- Access to high resolution figures
- Links to articles and content related to this article
- Copyright permission to reproduce figures and/or text from this article

View the Full Text HTML

The Spectral Elucidation versus the X-ray Structure of the Critical Precursor Complex in Bimolecular Electron Transfers: Application of Experimental/Theoretical Solvent Probes to Ion-Radical (Redox) Dyads

Sergiy V. Rosokha, Marshall D. Newton, Almaz S. Jalilov, and Jay K. Kochi*

Department of Chemistry, University of Houston, Houston, Texas 77204, and Department of Chemistry, Brookhaven National Laboratory, Upton, New York 11973

Received August 31, 2007; E-mail: jkochi@uh.edu

Abstract: The mechanistic conundrum is commonly posed by the intrinsic structural disconnect between a bimolecular (reactive) intermediate that is fleetingly detected spectroscopically in solution versus that rigorously defined by isolation and X-ray crystallography. We resolve this ambiguity by the combined experimental and theoretical application of the solvent media probe to the transient (1:1) precursor complex in the simplest chemical reaction involving direct adiabatic electron transfer (ET) among various donor/acceptor pairs. Of particular help in our resolution of such an important ET problem is the characterization of the bimolecular precursor complex as Robin−Day class II (localized) or class III (delocalized) from either the solvent-dependent or the solvent-independent response of the diagnostic intervalence absorption bands for the quantitative evaluation of the electronic coupling elements. The magnitudes of these intracomplex bindings are confirmed by theoretical (ab initio and DFT) computations that derive from X-ray structures and Marcus−Hush theories. Most importantly, the experimental solvent-induced ET barriers evaluated from the intervalence absorption bands are also quantitatively verified by the calculated outer-shell reorganization energies to establish unambiguously the intimate interconnection between the loosely bound bimolecular intermediate identified concurrently in solution and in the solid state.

---

1. Introduction

Classical descriptions of bimolecular reactions in solution proceed from the initial encounter of freely diffusing species to afford transient "collision" complexes. In the case of the conceptually simplest chemical reaction involving one-electron transfer (ET) between redox dyads: D (donor) and A (acceptor), the labile intermediate is commonly referred to as the 1:1 encounter or precursor complex [D,A];[1] and the second-order rate according to Marcus theory[2] is largely limited by the unimolecular ET transformation within the precursor complex, i.e.

$$D + A \underset{\text{(diff.)}}{\rightleftharpoons} [D,A] \underset{\text{ET}}{\rightleftharpoons} [D^{+\bullet},A^{-\bullet}] \underset{\text{(diff.)}}{\rightleftharpoons} D^{+\bullet} + A^{-\bullet} \quad (1)$$

Quantitative analyses of intermolecular ET mechanisms have mostly focused on outer-sphere ET processes[3] in which the electronic coupling or binding energy within the elusive

precursor complex is weak, with $H_{DA} < 200$ cm^{-1} so that the structural features of the reactants (D and A) and the products (D$^{+\bullet}$ and A$^{-\bullet}$) can be employed computationally, for the most part intact − and this choice thus simply circumvents any recourse to the labile encounter complex. However, there exists a large and growing number of intermolecular ET processes that occur at second-order rates which are faster than can be accommodated by non-adiabatic (or weakly adiabatic)[4,5] Marcus theory, and in some of these cases, circumstantial evidence points to the participation of transient precursor complexes that are responsible for the significantly lower ET barriers.[6,7] However, identification of the definitive structural parameters inherent to such strongly coupled precursor complexes has not been forthcoming, and their contribution to the attenuation of the ET barriers has not been rigorously established.

In earlier studies,[6−8] we found the existence of two independent procedures for the observation and characterization of the

---

(1) (a) Sutin, N. In *Bioinorganic Chemistry*; Eichhorn, G. L., Ed.; Elsevier: New York, 1973; Vol. 2, Chapter 19, p 611. (b) Cannon, R. D. *Electron Transfer Reactions*; Butterworth: London, 1980. (c) Newton, M. D.; Sutin, N. *Ann. Rev. Phys. Chem.* **1986**, *35*, 435. (d) Astruc, D. *Electron Transfer and Radical Processes in Transition-Metal Chemistry*; VCH: New York, 1995. (e) Gray, H. B., Winkler, J. R., Eds. *Electron Transfer in Chemistry*; Balzani, V., Ed.; Biological Systems, Vol. 3; Wiley-VCH: New York, 2001.

(2) Marcus, R. A.; Sutin, N. *Biochim. Biophys. Acta* **1985**, 811, 265. (b) Marcus, R. A. *Angew. Chem., Int. Ed. Engl.* **1993**, *32*, 1111. (c) Marcus, R. A. *Rev. Mod. Phys.* **1993**, *65*, 599.

(3) (a) Brown, G. M.; Sutin, N. *J. Am. Chem. Soc.* **1979**, *101*, 883. (b) Sutin, N. *Prog. Inorg. Chem.*, **1983**, *30*, 441.

(4) (a) Taube, H. *Electron-Transfer Reactions of Complex Ions in Solution*; Academic Press: New York, 1970. (b) Haim, A. *Prog. Inorg. Chem.* **1983**, *30*, 273. (c) Endicott, J. F.; Kumar, K.; Ramasami, T.; Rotzinger, F. P. *Prog. Inorg. Chem.* **1983**, *30*, 141−187.

(5) (a) Schwarz, C. L.; Endicott, J. F. *Inorg. Chem.* **1995**, *34*, 4572. (b) Formosinho, S. J.; Arnaut, L. G.; Fausto, R. *Prog. Reaction Kinetics* **1998**, *23*, 1.

(6) Ganesan, V.; Rosokha, S. V; Kochi, J. K. *J. Am. Chem. Soc.* **2003**, *125*, 2559.

(7) Rosokha, S. V.; Newton, M. D.; Head-Gordon, M.; Kochi, J. K. *Chem. Phys.* **2006**, *326*, 117.

(8) (a) Rosokha, S. V.; Kochi, J. K. *J. Am. Chem. Soc.* **2007**, *129*, 828. (b) Rosokha, S. V.; Kochi, J. K. *J. Am. Chem. Soc.* **2007**, *129*, 3683.

Chart 1

Electron Donor (D):
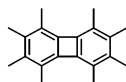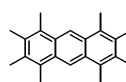
OMB   OMA   TTF

Electron Acceptor (A):

TCNE   DDQ   DBQ

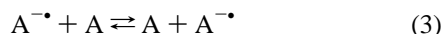bimolecular intermediates in the reversible ET self-exchange of electron donors (D) with their associated cation radicals, i.e.

$$D + D^{+\bullet} \rightleftarrows D^{+\bullet} + D \qquad (2)$$

and likewise with organic acceptors (A), i.e.

$$A^{-\bullet} + A \rightleftarrows A + A^{-\bullet} \qquad (3)$$

in which the formation of the reactive (donor/acceptor) intermediate according to eq 1 is represented by the 1:1 bimolecular associates: $[D,D^{+\bullet}]$ and $[A^{-\bullet},A]$, respectively. First, the transient (1:1) precursor complex is spectrally identified and characterized in solution by the appearance of its distinctive intervalence (or charge-transfer) absorption band.[6-9] Second, the 1:1 ion-radical associate is isolated under the experimental conditions of the ET self-exchange and then structurally scrutinized by single-crystal X-ray analysis — all under carefully controlled low-temperature conditions.

We now face the difficult mechanistic challenge of unambiguously bridging the dichotomous spectroscopic detection/identification of the *precursor complex in solution* versus the X-ray characterization of the *ion-radical associates in the solid state* by employing the following strategy based on Marcus−Hush theories.[2,10−12] In section 2.1., the quantitative solvent probe is used to establish the intermolecular (1:1) precursor complex as belonging to class II (localized) or class III (delocalized) according to the Robin−Day classification[13−15] by either the solvent-dependent or solvent-independent response of their diagnostic intervalence absorption bands.[16] In 2.2., we establish the definitive X-ray structures of the pertinent ion-

radical associates: $[D,D^{+\bullet}]$ and $[A^{-\bullet},A]$ as the loosely bonded bimolecular intermediates from the self-exchange in eqs 2 and 3, respectively. In 2.3., we depend on the X-ray structures of various ion-radical associates to calculate the electron-transfer parameters: λ_T (reorganization energy) and H_{DA} (electron coupling element) with the aid of Marcus[10] and Hush[11] theories for both Robin−Day class II and class III intermediates, and to establish how each responds to changing solvent environments, irrespective of their overall charge. In this way, we hope to demonstrate how the intimate interplay between experiment (X-ray, NIR) versus theoretical computation (λ_T, H_{DA}) can be used to mutually reinforce the validation of otherwise disparate mechanistic concepts in solution versus the crystalline (solid) state.

2. Results and Discussion

For this study of ET self-exchange, we focus on three pairs of electron donors and acceptors depicted in Chart 1, together with their acronyms for ready identification.

Our first aim is to establish the localized or delocalized nature of the intermolecular precursor complexes $[D,D^{+\bullet}]$ and $[A^{-\bullet},A]$ and to evaluate the electron-transfer parameters for such cationic and anionic associates.

2.1. Spectral Characterization of the Precursor Complexes of Ion Radicals and their Diamagnetic Parents in Various Solvents and their Assignment as Robin−Day Class II or Class III. The cation radicals of the donors (D) in Chart 1 were prepared with a non-coordinating counteranion as pure uniunivalent salts: $D^{+\bullet} CB^-$, where CB^- represents the bulky *closo*-dodeca-methyl-carboranate.[8] Likewise, the anion radicals ($A^{-\bullet}$) of the acceptors were prepared as the crystalline salts: $M(L)^+A^{-\bullet}$, in which the non-coordinating countercation was an alkali metal (M^+) either encapsulated within the cavity of [2,2,2]cryptand or sandwiched between a pair of crown-ether ligands (L).[17] Such a choice assured the solubility of these salts in various organic solvents of different polarity; and the persistency of the ion radicals in these solutions was always sufficient for quantitative spectral measurements with minimal ion-pairing effects between the cation/anion radicals and their bulky (delocalized) counterions.[18]

(9) (a) Badger, B.; Brocklehurst, B. *Nature* **1968**, *219*, 263. (b) Badger, B.; Brocklehurst, B. *Trans. Faraday Soc.* **1969**, *65*, 2582; Badger, B.; Brocklehurst, B. *Trans. Faraday Soc.* **1970**, *66*, 2939.
(10) (a) Marcus, R. A. *Discuss. Faraday Soc.* **1960**, *29*, 21. (b) Marcus, R. A. *J. Phys. Chem.* **1963**, *67*, 853. (c) Marcus, R. A. *J. Chem. Phys.* **1965**, *43*, 679.
(11) (a) Hush, N. S. *Prog. Inorg. Chem.* **1967**, *8*, 391. (b) Hush, N. S. *Electrochim. Acta* **1968**, *13*, 1005.
(12) (a) Newton, M. D. *Chem. Rev.* **1991**, *91*, 767. (b) Creutz, C.; Newton, M. D.; Sutin, N. *J. Photochem. Photobiol., A* **1994**, *82*, 47. (c) Brunschwig, B. S.; Sutin, N. In *Electron Transfer in Chemistry*; Balzani, V., Ed.; Wiley: New York, 2001; Vol. 2, p 583. (d) Brunschwig, B. S.; Sutin, N. *Coord. Chem. Rev.* **1999**, *187*, 233. (e) Sutin, N. *Adv. Chem. Phys.* **1999**, *106*, 7. (f) Brunschwig, B. S.; Creutz, C.; Sutin, N. *Chem. Soc. Rev.* **2002**, *31*, 168.
(13) Robin, M. B.; Day, P. *Adv. Inorg. Chem. Radiochem.* **1967**, *10*, 247.
(14) Although the Robin−Day classification was originally based on D−bridge−A or intramolecular mixed-valence complexes,[12] the theoretical and experimental basis for its application to intermolecular (through-space) systems has been established.[15]
(15) (a) Sun, D.-L.; Rosokha, S. V.; Lindeman, S. V.; Kochi, J. K. *J. Am. Chem. Soc.*, **2003**, *125*, 15950, (b) Sun, D.-L.; Rosokha, S. V.; Kochi, J. K. *J. Am. Chem. Soc.* **2004**, *126*, 1388.
(16) (a) The solvent-dependent behavior of the intervalence absorption band was established for class II (as opposed to class III) intramolecular mixed-valence systems,[16b] and it is employed here for the first time since the theoretical interpretation of the intervalence band applies equally to intramolecular as well as intermolecular electron transfers.[12,15] (b) Creutz, C. *Prog. Inorg. Chem.* **1983**, *30*, 1.
(17) (a) Davlieva, M. G.; Lü, J. M.; Lindeman, S. V.; Kochi, J. K. *J. Am. Chem. Soc.*, **2004**, *126*, 4557. (b) Lu, J. M.; Rosokha, S. V.; Lindeman, S. V.; Neretin, I. S.; Kochi, J. K. *J. Am. Chem. Soc.* **2005**, *127*, 1797.
(18) Rosokha, S. V.; Lu, J. M.; Newton, M. D.; Kochi, J. K. *J. Am. Chem. Soc.* **2005**, *127*, 7411.
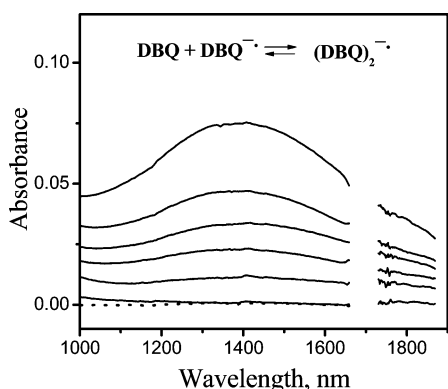
Figure 1. Intervalence absorption in the NIR spectral range upon the addition of **DBQ** acceptor to the 2.6 mM solution of Na(cryptand)$^+$**DBQ**$^{-•}$ in PC. Concentration of **DBQ** (solid lines from bottom to top, in mM): 0, 2, 4, 6, 10, 18. [Note the dotted line represents the spectrum of **DBQ** alone.]
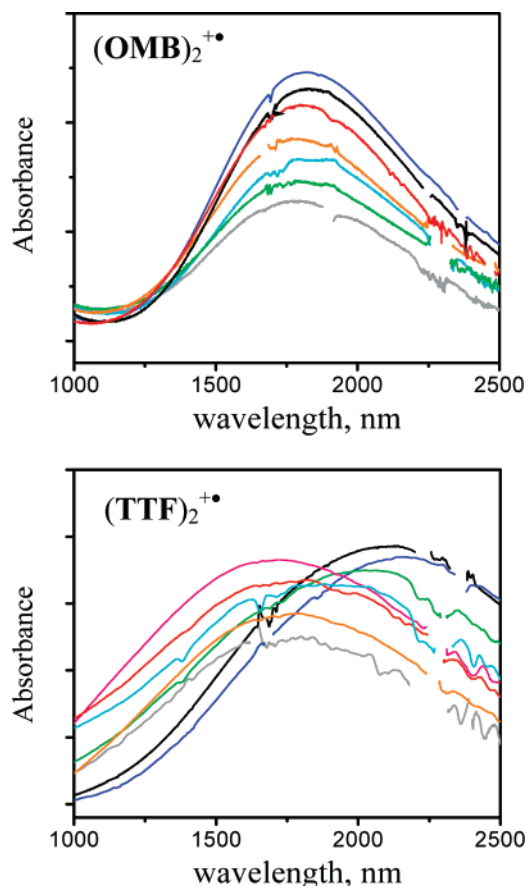

Figure 2. Electronic (NIR) spectra of (**OMB**)$_2$$^{+•}$ (top) and (**TTF**)$_2$$^{+•}$ (bottom) measured in: CHCl$_3$ (blue), CH$_2$Cl$_2$ (black), acetone (red), CH$_3$CN (orange), THF (light blue), diethyl ether (green), PC (gray), and DMF (pink) [Note that the absorption intensities are presented in arbitrary units and normalized with respect to λ_{max}.]

The electronic spectra of the donors or acceptors in Chart 1 as well as their ion radicals were uniformly transparent in the near-IR range (between 1000−3000 nm). However, as reported earlier, the addition of the parent donor or acceptor to the dichloromethane solution of corresponding ion radicals (or vice versa) resulted in the appearance of new absorption bands in the near-IR range (1000−2500 nm).[7,8] Previous quantitative analysis of the dependence of such NIR intensities on the temperature as well as the concentration of the ion radicals and
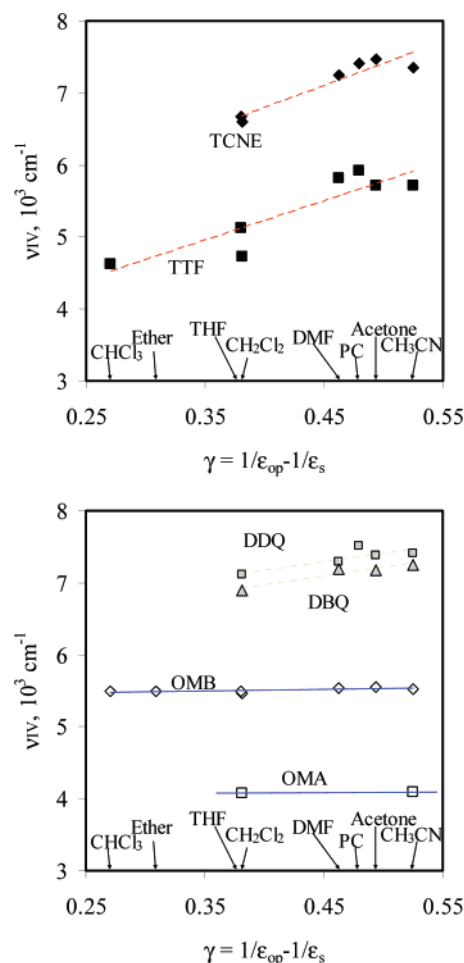
Figure 3. Solvent dependence of the intervalence transition energy for various ion-radical associates.

their neutral counterparts led to assignment of these characteristic absorptions to the intervalence (or charge-resonance)[9,11,19] transition of the precursor complex with [D,A] = [D,D$^{+•}$] and [A$^{-•}$,A] according to eq 1.

Similar appearances of the intervalence absorption bands were observed when the same ion radicals were mixed with their diamagnetic parents in the other solvents. For example, Figure 1 typically illustrates the NIR spectral changes indicative of the formation of (**DBQ**)$_2$$^{-•}$ as the bimolecular associate in propylene carbonate (PC). Spectral maxima of these positively and negatively charged precursor complexes in the NIR range are listed in Table 1 in various solvents together with their formation constants (K_{DA}) based on eq 1.

Even a cursory glance at the data in Table 1 reveals that the NIR bands of the various precursor complexes are subject to quite different solvent perturbations. For example, as illustrated in Figure 2, the intervalence transition for the (**OMB**)$_2$$^{+•}$ complex (upper) is essentially invariant in various solvents, whereas that of the (**TTF**)$_2$$^{+•}$ complex (lower) is blue-shifted in acetonitrile or acetone compared to that observed in the less polar dichloromethane or chloroform.

---

(19) Historically, the electronic transitions associated with such [D,D$^{+•}$] complexes of aromatic π-donors and their cation radicals have been referred to as charge-resonance absorptions.[9] On the other hand, the absorptions related to the vertical electron transfer within donor/acceptor redox pairs have been referred to as charge-transfer bands[33] and as intervalence bands for mixed-valence complexes.[11] Accordingly to avoid confusion, hereinafter all these optical transitions will be uniformly referred to as *intervalence*.

Table 1. Intervalence Absorption Band (λ_{IV}, nm) and the Formation Constant (K_{DA}, M^{-1}, in parenthesis) of Various Cationic and Anionic Precursor Complexes in Different Solvents[a]

solvent	(OMB)$_2^{+\bullet b}$	(OMA)$_2^{+\bullet}$	(TTF)$_2^{+\bullet}$	(TCNE)$_2^{-\bullet}$	(DDQ)$_2^{-\bullet}$	(DBQ)$_2^{-\bullet}$
CH$_2$Cl$_2$	1830 (350)[f]	2430 (60)[f]	2115 (6)[d]	1515 (4.5)[e]	1406 (11)[f]	1450
THF	1820 (50)	c	1950 (0.4)[d]	1500 (0.4)[e]	c	c
PC[a]	1800	c	1760	1356	1356	1400
acetone	1812 (110)	c	1750 (0.6)[d]	1360 (0.3)[e]	1349	1380
CH$_3$CN	1805 (100)	2426	1720 (0.7)[d]	1380 (1.0)[e]	1372	1390
DMF	c	c	1690 (0.3)[d]	1350[e]	1335	c
CHCl$_3$	1820	c	2160	c	c	c

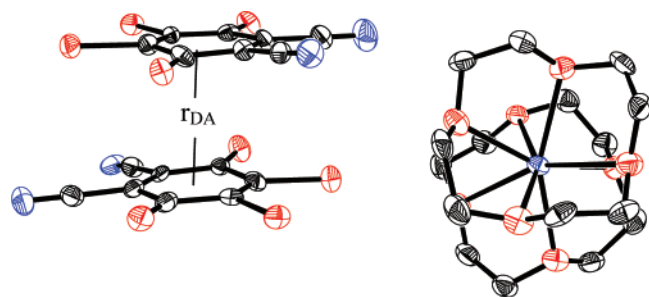[a] Measured at 295 K. [b] Extinction coefficients at λ_{IV} are $(5 \pm 1) \times 10^3$ M^{-1} cm^{-1} in all solvents. [c] Reliable measurements of complex formation were hindered by either reactant solubility, side reactions, or solvent interference. [d] Reference 8a. [e] Reference 7. [f] Reference 8b.

The solvent effects on the spectral data from Table 1 are graphically summarized in Figure 3 in which the transition energies of the NIR bands for each ion-radical complex are plotted as the function of the solvent Pekar factor γ.[10] Note that the choice of abscissa with $\gamma = 1/\epsilon_\infty - 1/\epsilon_0$ taken as the quantitative solvent characteristic is based on the two-sphere Marcus expression for the solvent reorganization energy:[2,10,20]

$$\lambda_o = (1/\epsilon_\infty - 1/\epsilon_o) \times (\Delta q)^2 (1/2r_D + 1/2r_A - 1/r_{DA}) \quad (4)$$

where ϵ_∞ and ϵ_o are optical and static dielectric constants, Δq is the transferred charge, r_D and r_A are effective molecular radii of the donor and acceptor, and the r_{DA} is the electron-transfer distance.

The striking feature in Figure 3 is the clear differentiation of the various precursor complexes into those that are (top) and those that are not (bottom) subject to measurable solvent perturbation, irrespective of the positive or negative charge they bear.

The consideration of Figure 3 allows us to clearly differentiate the precursor complexes into three categories. Thus, (OMB)$_2^{+\bullet}$ and (OMA)$_2^{+\bullet}$ are characterized by reasonably solvent-independent behavior of the NIR bands. In strong contrast, (TTF)$_2^{+\bullet}$ and (TCNE)$_2^{-\bullet}$ both suffer significant variations of the NIR bands in different solvents as measured by a roughly linear relationship between ν_{IV} and γ in Figure 3 (top).[20] Inbetween lie (DDQ)$_2^{-\bullet}$ and (DBQ)$_2^{-\bullet}$ in which the variation of the intervalence band with solvent consistently exists in a rather narrow range, and any solvent-induced change is, at best, considered problematic. Further comparisons of the data from Table 1 also reveal that the formation constants for (OMB)$_2^{+\bullet}$ and (OMA)$_2^{+\bullet}$ are notably higher than those of the other precursor complexes.[21] Moreover, the largest values of K_{DA} were uniformly measured in dichloromethane for all bimolecular complexes.

The distinctive delineation of the precursor complex into two limiting types of solvent behavior in Figure 3 accords with their identification as either a Robin–Day class II or III complex, as well as a borderline class II/III.[22] The stabilization of such bimolecular associates is achieved by intracomplex electronic

Chart 2

$$[D, D^{+\bullet}] \rightleftharpoons [D^{+\bullet}, D] \qquad versus \qquad [D, D^{+\bullet}] \leftrightarrow D^{+\bullet}, D]$$

Class II (localized)   Class III (delocalized)

coupling—the magnitude of which determines whether the unpaired electron can hop (dynamic) or is delocalized (static) between the pair of redox centers, as pictorially depicted in Chart 2.[23]

As such, the potential-energy surface of the class II complex will consist of a pair of degenerate minima, and the intervalence transition will be subject to solvent perturbation, whereas the class III complex with a single minimum is not.[12]

2.2. X-ray Structures of Ion-Radical Associates as Crystalline Guides to Class II and III Behavior. The slow diffusion of hexane into an equimolar solution of Na(12crown4)$_2^+$(**DBQ**)$^{-\bullet}$ and **DBQ** in dichloromethane at -60 °C resulted in the formation of the dark-brown crystals, the X-ray analysis of which shows the monoclinic unit cell to contain a pair of close-lying **DBQ** moieties, together with the sodium counterion sandwiched between a pair of 12-crown-4 polyether ligands (Figure 4). [For the X-ray structure of the parent acceptor **DBQ** and anion-radical salt: Na(12crown4)$_2^+$(**DBQ**)$^{-\bullet}$, see the Supporting Information.] Table 2 compares the bimolecular structure of the (**DBQ**)$_2^{-\bullet}$ associate with the corresponding X-ray structures of the ion-radical associates listed in Chart 1 together with others reported earlier.[7,8,24,25] The detailed consideration of the X-ray structure of the (**DBQ**)$_2^-$ associate in Figure 4 revealed two important features, as follows:

2.2.1. The presence of distinct (**DBQ**)$_2^{-\bullet}$ dyads in which the pair of donor/acceptor moieties lie parallel at the relatively long-

(20) (a) Note that Figure 2 is merely presented for the qualitative illustration of the contrasting solvent dependence (or independence) of the intervalence absorption bands of different complexes. The choice of the Pekar factor as abscissa is a common practice,[38] and it is not intended for the quantitative verification of the Marcus two-sphere dielectric continuum model (which is not appropriate for our systems, vide infra). (b) Figure 3 (top) illustrates the significant solvent dependence of the observed intervalence transitions of both the cationic (**TTF**) and anionic (**TCNE**) complexes—in contrast to the essentially solvent-independent (or weakly dependent) spectra of cationic and anionic complexes shown in the Figure 3 (bottom). As such, we conclude that the observed difference among the various complexes is not related to the charge they bear.

(21) Note also that low-temperature ESR and electrochemical studies of (**OMB**)$_2^{+\bullet}$ reveal doubled ESR spectra (in comparison to those of monomer ion radicals) that are characteristic of completely delocalized dimeric species.[21b] Furthermore, the splitting of the electrochemical oxidation wave[8b] also indicates the facile formation of the (**OMB**)$_2^{+\bullet}$ complex with strong electronic coupling between octamethylbiphenylene moieties. By contrast, only temperature- and concentration-dependent ESR line-broadening (resulting from intermolecular self-exchange electron transfer) and a single CV wave have been observed for class II systems over a wide range of temperatures. (b) Kochi, J. K.; Rathore, R.; Le Magueres, P. *J. Org. Chem.* **2000**, *65*, 6826.

(22) For other examples of borderline class II/III complexes, see: (a) Demadis, K. D.; Hartshorn, C. M.; Meyer, T. J. *Chem. Rev.* **2001**, *101*, 2655. (b) Dinolfo, P. H.; Lee, S. J.; Coropceanu, V.; Bredas, J.-L.; Hupp, J. T. *Inorg. Chem.* **2005**, *44*, 5789. (c) Nelsen, S. F.; Konradsson, A. E.; Telo, J. P. *J. Am. Chem. Soc.* **2005**, *127*, 920. (d) D'Alessandro, D. M.; Topley, A. C.; Davies, M. S.; Keene, F. R. *Chem. Eur. J.* **2006**, *12*, 4873. (e) Nelsen, S. F.; Weaver, M. N.; Telo, J. P. *J. Am. Chem. Soc.* **2007**, *129*, 7036.

(23) For more extended discussions and illustrations of this important point, see: Rosokha, S. V.; Neretin, I. S.; Sun, D.-L.; Kochi, J. K. *J. Am. Chem. Soc.* **2006**, *128*, 9394.

(24) (a) Marsh, R. E. *Acta Crystallogr., Sect. B* **1999**, *55*, 931. (b) Rathore, R.; Kumar, A. S.; Lindeman, S. V.; Kochi, J. K. *J. Org. Chem.* **1998**, *63*, 5847.

(25) (a) Yakushi, K.; Nishimura, S.; Sugano, T.; Kuroda, H. *Acta Crystallogr., Sect. B* **1980**, *36*, 358. g) Le Magueres, P. Lindeman, S.V.; Kochi, J.K. *Org. Lett.* **2000**, 3567.

Figure 4. ORTEP diagram of the ion-radical associate as the crown ether ligated sodium salt: $Na(12crown4)_2{}^+(\mathbf{DBQ})_2{}^{-\bullet}$.

bonded distance of $r_{DA} = 3.03$ Å (and slightly shifted laterally along the main axis). The fact that r_{DA} is significantly less (by ~ 0.4 Å) than the sum of the van der Waals radii augurs the presence of a strong (noncovalent) bonding interaction between the pair of **DBQ** counterparts. The structure of the $(\mathbf{DBQ})_2{}^{-\bullet}$ associate in Figure 4 is highly reminiscent of the X-ray structures of a number of other ion-radical associates, both positively and negatively charged, with the common basic structural or bonding motif in which the D and D^+ dyads (as well as the $A^{-\bullet}$ and A dyads) consistently lie coplanar in a rather narrow range of interplanar π-separations, i.e., $r_{DA} = 3.1 \pm 0.3$ Å.[8,24,25] Moreover the "intermolecular" structures of the ion-radical associates identified in Table 2 can experience minor variations from the vertical π-stacking (as illustrated for $(\mathbf{TTF})_2{}^{+\bullet}$ in entry 7) that involve either slight slippages along the horizontal plane (as in Figure 4) or rotation around the vertical axis (as illustrated for $(\mathbf{NAP})_2{}^{+\bullet}$ in the last entry); however, such conformational variants do not seem to impose a significant energy penalty.[8]

2.2.2. The average values of the corresponding C–C bond lengths in both DBQ moieties lie within the accuracy limit of the X-ray measurements. Thus, in two independent **DBQ** molecules, the average values of the C=O bonds are 1.228 and 1.229 Å, respectively, and the average values of the C=C bonds are 1.364 and 1.367 Å. Since these bond lengths provide the structural measure of the charge residing on the quinonoid centers,[26,27] such an equivalency reveals the existence of almost equal (negative) charge distribution ($-0.5/-0.5$) between both moieties within the $(\mathbf{DBQ})_2{}^{-\bullet}$ associate that is indicative of the bimolecular (Robin–Day) class III complex.[28] A similar charge (electron) distribution is also observed in $(\mathbf{DDQ})_2{}^{-\bullet}$ and $(\mathbf{TCNQ})_2{}^{-\bullet}$ among anionic (ion-radical) associates, as well as in the cationic associates: $(\mathbf{OMA})_2{}^{+\bullet}$, $(\mathbf{OMB})_2{}^{+\bullet}$ and $(\mathbf{NAP})_2{}^{+\bullet}$.[8,24,25] Contrastingly, the X-ray structures in different crystalline $(\mathbf{TTF})_2{}^{+\bullet}$ modifications can be construed as class II,[8,29] but the extensive multiple π-stacking arrangements discourage a definitive X-ray assignment. [Owing to the weaker electronic coupling in $(\mathbf{TTF})_2{}^{+\bullet}$, we were unable to isolate the

discrete binary form of this bimolecular cation, as well as that of the related anionic associate of **TCNE**.[30]]

Let us now consider how the X-ray structures of the intermolecular ion-radical associates are critical to the evaluation/calculation of the electron-transfer parameters: λ_T (reorganization energy) and H_{DA} (electronic coupling) of class II and class III complexes.

2.3. Theoretical Evaluation of the ET parameters (H_{DA} and λ_T) from the X-ray Structures of Class II and III Precursor Complexes: Applicability of Marcus–Hush Two-State Theory. Initially, the quantitative applicability of theoretical electron-transfer models was examined in the structural interconnection between the precursor complex elucidated in solution via their diagnostic intervalence transitions versus the ion-radical associates independently identified by X-ray analysis (Table 2).

2.3.1. Quantitative Comparisons of the Experimental and Theoretical Electronic Coupling Energies (H_{DA}). Theoretical evaluation of the electronic coupling element for $[D^{+\bullet},D]$ and $[A,A^{-\bullet}]$ was based on the energy splitting resulting from the symmetric and antisymmetric combinations of the localized molecular orbitals of the constituent monomers upon association to the neutral dimer at the (in vacuo) ab initio Hartree–Fock level with the 6-311G* basis set and by DFT calculations (B3LYP).[12a,31,32] For the cationic compplexes $[D,D^{+\bullet}]$, the orthogonal coordinates based on the X-ray structures in Table 2 were taken for the computations of the orbital energies, and one-half the difference of the HOMO–1 and HOMO (highest symmetric and antisymmetric occupied orbitals) energies resulting from these computations of neutral dimers corresponded to the values of the coupling elements H_{DA} for $[D^{+\bullet},D]$ listed in Table 3. In a similar way, the experimental X-ray structures of the anionic associates $[A,A^{-\bullet}]$ were used in the computations of the orbital energies of the corresponding neutral closed-shell dimers, and one-half the energy difference between LUMO and LUMO+1 that resulted from these computations (i.e., the energies of the lowest symmetric and antisymmetric virtual orbitals) led to the values of H_{DA} for $[A,A^{-\bullet}]$ in Table 3 (see Table S2 in Supporting Information for details of these calculations).

The independent experimental evaluation of H_{DA} for the localized class II complexes $(\mathbf{TTF})_2{}^{+\bullet}$ and $(\mathbf{TCNE})_2{}^{-\bullet}$ were obtained from the Mulliken–Hush treatment[11,33] of the intervalence optical transition (ν_{IV}), i.e.

(26) Lindeman, S. V.; Rosokha, S. V.; Sun, D.; Kochi, J. K. *J. Am. Chem. Soc.* **2002**, *124*, 843.

(27) Lu, J. M.; Rosokha, S. V.; Neretin, I. S.; Kochi, J. K. *J. Am. Chem. Soc.* **2006**, *128*, 16708.

(28) Sun, D.-L.; Rosokha, S. V.; Kochi, J. K. *J. Phys. Chem. B* **2007**, *111*, 6655.

(29) (a) Kondo, K.; Matsubayashi, G.; Tanaka, T.; Yoshioka, H.; Nakatsu, K. *J. Chem. Soc. Dalton* **1984**, 379. (b) Legros, J.-P.; Bousseau, M.; Valade, L.; Cassoux, P. *Mol. Cryst. Liq. Cryst.* **1983**, *100*, 181.

(30) (a) Owing to the weakly coupled nature of $(\mathbf{TCNE})_2{}^{-\bullet}$ and $(\mathbf{TTF})_2{}^{+\bullet}$, none of the crystalline modifications of the ion-radical associates exist as binary units bearing a distinctive (-1) or ($+1$) charge. (b) For the structures of $(\mathbf{TCNE})_2{}^{-\bullet}$ and $(\mathbf{TTF})_2{}^{+\bullet}$ used in the calculations, see the discussion by Rosokha et al. in refs 7 and 8a.

(31) Pople, J. A.; et al. *Gaussian 98*, Revision A.11.3 ed.; Gaussian, Inc.: Pittsburgh, PA, 2001. Complete ref in Supporting Information.

(32) (a) Newton, M. D. In *Electron Transfer in Chemistry*; Balzani, V., Ed.; Wiley-VCH: New York, 2001; Vol. 1, p 3. (b) Huang, J.-S.; Kertesz, M. *J. Chem. Phys.* **2005**, *122*, 234707.

(33) Mulliken, R. S.; Person, W. B. *Molecular Complexes*; Wiley: New York, 1969.

(34) Note that the ground-state adiabatic minima for borderline class III/II complexes approach $X = 0.5$. Accordingly, these electronic transitions involve little (if any) charge transfer, and their energies are largely determined by the value of coupling element with minimal contribution of the reorganization energy. This applies even when these compounds are (strictly speaking) localized, and their transition energy can be mathematically related to the diabatic reorganization energy (see the discussion in ref 12).

Table 2. X-ray Structures of Ion-Radical Associates and Their Interplanar Separations (r_{DA})

Dyads	Structure	r_{DA},[a] Å	Dyads	Structure	r_{DA},[a] Å
(DBQ)$_2$$^{-\bullet}$		3.03	**(OMB)$_2$$^{+\bullet}$**		3.40[e]
(DDQ)$_2$$^{-\bullet}$		2.95[b]	**(OMA)$_2$$^{+\bullet}$**		3.37[f]
(TCNE)$_2$$^{2-}$		2.88[c]	**(TTF)$_2$$^{2+}$**		3.40[g]
(TCNQ)$_2$$^{-\bullet}$		3.17[d]	**(NAP)$_2$$^{+\bullet}$**		3.17[h]

[a] The values of r_{DA} represent the average deviations of the core atoms of one monomer (i.e., naphthalene, biphenylene, anthracene, the quinones, and tetrathiafulvalene) from the best least-squares plane (calculated by the XP crystallographic program) through the same atoms of the other monomer. The monomers lying within the **(OMA)$_2$$^{+\bullet}$**, **(OMB)$_2$$^{+\bullet}$**, **(NAP)$_2$$^{+\bullet}$**, **(DDQ)$_2$$^{-\bullet}$**, and **(TCNQ)$_2$$^{-\bullet}$** complexes are crystallographically symmetric, and the corresponding planes are parallel. The dihedral angles subtending the planes of the crystallographically independent monomers of **(TTF)$_2$$^{+\bullet}$** (0.4°) and **(DBQ)$_2$$^{-\bullet}$** (1.1°) are negligible. [b] Reference 8b. [c] Reference 7b. [d] Reference 24a. [e] Reference 24b. [f] Reference 21b. [g] Reference 25a. [h] Reference 25b.

Table 3. Comparison of the Theoretical[a] and Spectral[b] Evaluations of the Coupling Elements

complex	ν_{IV},[c] 10^3 cm^{-1}	class	H_{DA} (spectral), 10^3 cm^{-1} [b]	H_{DA}(theor),[a] 10^3 cm^{-1}
(OMB)$_2$$^{+\bullet}$	5.46−5.60	III	2.	2.3 (3.2)[d]
(OMA)$_2$$^{+\bullet}$	4.08−4.09	III	2.0	1.5 (2.1)
(TTF)$_2$$^{+\bullet}$ [c]	4.65−5.92	II	(1.6)[e]	3.6[e] (4.8)
(NAP)$_2$$^{+\bullet}$	9.5[f]	III	4.8	4.6 (6.3)
(TCNE)$_2$$^{-\bullet}$	6.60−7.41	II	(1.1)[d]	4.2 (7.2)[d]
(DDQ)$_2$$^{-\bullet}$	7.30−7.56	II(III)	3.7 (1.8)[d]	3.4 (4.8)[d]
(DBQ)$_2$$^{-\bullet}$	6.90−7.25	II(III)	3.5 (1.8)	2.9 (4.3)
(TCNQ)$_2$$^{-\bullet}$	4.5[g]	II(III)	2.3 (1.4)	1.9 (3.3)

[a] DFT (B3LYP) or Hartree−Fock (in parenthesis) calculation with 6-311G* basis set as described in text. [b] As $H_{DA} = \nu_{IV}/2$ (for class III and borderline class II/III complexes); in parenthesis: $H_{DA} = 0.0206(\nu_{IV} \Delta\nu_{1/2} \epsilon_{IV})^{1/2}/r_{DA}$ (for class II and borderline class II/III complexes). [c] Average variation of the intervalence transition energies in different solvents. [d] Reference 8b. [e] Reference 8a. [f] Reference 21b. [g] Reference 8b.

$$H_{DA} = 0.0206(\nu_{IV} \Delta\nu_{1/2} \epsilon_{IV})^{1/2}/r_{DA} \qquad (5)$$

where $\Delta\nu_{1/2}$ is the full-width at half-maximum (cm^{-1}) of the NIR absorption band, ϵ_{IV} is its extinction coefficient (M^{-1} cm^{-1}), and r_{DA} is the separation (Å) between the donor/acceptor centers. The NIR absorption data were simulated with Gaussian band-shapes together with the separation parameter taken from the X-ray structures. On the other hand, the experimental evaluation of H_{DA} in Table 3 (column 4) for the class III complexes **(OMB)$_2$$^{+\bullet}$** and **(OMA)$_2$$^{+\bullet}$** involving the complete (electron) delocalization between both redox centers, relied on the direct relationship between the transition energy and the electronic coupling element, i.e.

$$H_{DA} = \nu_{IV}/2 \qquad (6)$$

according to the Mulliken−Hush two-state model.[11,12,16b]

The analysis of the results in Table 3 allows us to draw several important conclusions: (1) For class III and borderline class II/III complexes,[22] the electronic coupling elements resulting from ab initio (DFT) computations were closely related to the experimental energies based on their intervalence NIR bands taken as $H_{DA} = \nu_{IV}/2$ (Figure 5). In fact, the values of coupling element obtained from NIR spectra were intermediate between the higher values resulting from Hartree−Fock computations and those from the DFT method.[8,32] Such a coincidence of H_{DA} values supports the applicability of the Marcus−Hush two-state model—especially to the intermolecular class III precursor complexes. (2) The values of the experimental electronic coupling elements determined via the Mulliken−Hush formalism for the class II and borderline class II/III complexes were somewhat lower than the theoretical values obtained from ab initio computations; however, such deviations were discussed earlier in terms of the uncertainty in the evaluation of the bimolecular separation parameter, r_{DA}.[35,36] In view of the labile nature of such intermolecular complexes in solution, it is not unreasonable to expect that H_{DA} will be easily modulated by dynamic equilibria around several isoenergetic structures.[37] It is particularly noteworthy that the largest discrepancy between the Mulliken−Hush and ab initio calculations were observed for **(TTF)$_2$$^{+\bullet}$** and **(TCNE)$_2$$^{-\bullet}$** in Table 3. The latter supports the thesis that the most pronounced deviations of the dynamic (solution) structures from solid-state structures lie with class II complexes—which suffer from the weakest electronic coupling interactions between monomers in such associates (see Table

(35) (a) Even for bridged donor/acceptor systems consisting of fixed redox centers, the proper value of this parameter was found to be lower by up to ~20−30% relative to that based on the simple (geometric) separation of redox centers.[36] (b) Note that the possible underestimation of the coupling element via the Mulliken−Hush analysis (eq 5) was also noted recently for bridged mixed-valence systems.[22e]
(36) Nelsen, S. F.; Newton, M. D. *J. Phys. Chem. A* **2000**, *104*, 10023.
(37) (a) For the possible existence of equilibrium mixtures of different types of isomeric conformers (such as those in Table 2 based on X-ray structures) of ion-radical associates that can lead to enhanced r_{DA} (and diminished H_{DA}) values in solution, see the discussion in Rosokha and Kochi in ref 8a. (b) Note that the theoretical calculations of H_{DA} indicate a strong dependence on the (vertical) interplanar separation (r_{DA}) and rather smaller (energy) effects imposed by conformational changes involving horizontal slippage or rotation (at constant r_{DA}).[8a]
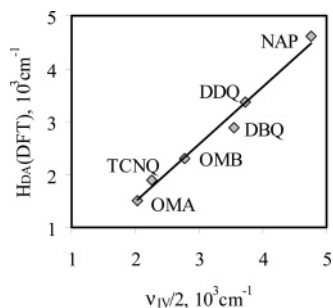
Figure 5. Concordance of the calculated (DFT) values of H_{DA} based on the HOMO−LUMO splitting with the experimental values from the NIR absorption band according to eq 6.[12,34]

3). Most importantly, the close correspondence shown in Figure 5 between the H_{DA} values obtained from the spectral data and those calculated on the basis of X-ray structures for the strongly bound class III and borderline class II/III systems confirms the conclusion that X-ray structures of ion-radical associates are valid surrogates for the bimolecular precursor complexes in solution.

2.3.2. Quantitative Treatment of Solvation from the Outer-Shell Reorganization Energies (λ_o) of Class II Complexes. The intrinsic barrier (λ_T) for electron transfer within the precursor complex in Scheme 1 (eq 1) according to Marcus theory is simply taken as the sum of the solvent-independent or inner-shell (λ_i) and solvent-dependent or outer-shell (λ_o) components.[2] Accordingly, attention to the solvatochromic effects that are experimentally displayed by the intervalence transitions in Figure 2 can be, in the first instance, directed to the role of the solvent. Indeed, the verification of the theoretically evaluated solvent dependence of λ_T (dominated by λ_o) has been the subject of intensive experimental and theoretical studies for *intramolecular* electron transfers in bridged donor/acceptor dyads in the form of both thermoneutral and nonthermoneutral exchanges in mixed-valence complexes.[38,39] However, analogous studies of precursor complexes pertinent *to bimolecular* electron transfers have been singularly missing heretofore owing to the paucity of adequate structural and spectral characterizations of such transient (encounter) complexes. Therefore, in order to lend theoretical credence to the experimental observations of marked solvent effects as noted in Table 1 and Figure 3, let us now quantitatively evaluate these reorganization barriers by applying Marcus−Hush theories based on the X-ray structures of the ion-radical associates in Table 2.[40]

The relevant solvent reorganization energies (λ_o) were determined within the framework of the dielectric continuum model (DCM) as the free energy of the inertial solvent response to a solute cavity containing either $[D^{+\bullet},D]$ or $[A,A^{-\bullet}]$:[41]

$$\lambda_o = G_s(\epsilon_{\infty 1},\epsilon_{\infty 2},...,\epsilon_{\infty N},\Delta\mathbf{q}) - G_s(\epsilon_{01},\epsilon_{02},...,\epsilon_{0N},\Delta\mathbf{q}) \quad (7)$$

where $\Delta\mathbf{q}$ is the point-charge representation of the full shift in the charge density in the donor/acceptor dyad upon electron transfer. Thus the limiting Marcus two-sphere model (TSM) for the reorganization energy λ_o in bimolecular ET as given by eq 4 is replaced by the general eq 7 in which the more realistic dielectric continuum framework is based on the full solution of the Poisson equation for the solute cavity of given size, shape, and charge distribution immersed in a solvent environment composed of several dielectric zones, each characterized by an ϵ_o, ϵ_∞ pair, and with due account taken of the boundary conditions at all interzone contacts.[42] For the cavity containing the precursor complex, the change in charge density is represented by the variation of the point charge (Δq_i) at each atomic site (i) of the molecular solute and the dielectric zones (N in number) are denoted by the second subscript for each ϵ in eq 7, and the atomic point charge shifts are represented by the vector $\Delta\mathbf{q}$.[43] In other words, eq 7 represents the outer-shell reorganization energy λ_o as the free energy of inertial solvent response to a solute with charge density $\Delta\mathbf{q}$. This solvent inertial response involves solvent nuclear polarization modes and is calculated as the difference between the optical response and the full response given as the first and the second term, respectively, in eq 7. [Indeed, such a difference is also implicit in the classical Marcus two-sphere model (eq 4) in which the solvation energies, G_s and λ_o are quadratic functions of Δq_i when the solute is linearly coupled to the solvent medium.]

The calculation of the reorganization energies λ_o for $(\mathbf{TCNE})_2^{-\bullet}$ and $(\mathbf{TTF})_2^{+\bullet}$ complexes based on eq 7 employed the Delphi Poisson solver[44] and a two-zone model. The high-frequency dielectric constant of 2 was denoted as ϵ_{in} ($\epsilon_{in} \equiv \epsilon_{o1} = \epsilon_{\infty 1}$) for assignment to the solute (zone 1) and the surrounding organic solvent ($\epsilon_o \equiv \epsilon_{o2}$ and $\epsilon_\infty \equiv \epsilon_{\infty 2}$) represented zone 2. The value $\epsilon_{in} = 2$ mimicked the solute polarizability and was deemed appropriate for solute charges obtained from the calculations of the separate isolated species and then subjected to a solvent reaction field.[45] The Δq_i values were evaluated as the difference between corresponding ESP atomic charges calculated for the isolated neutral **TCNE** and **TTF** molecules and **TCNE**$^{-\bullet}$ and **TTF**$^{+\bullet}$ ion radicals.[7,8] These ESP charges (as fitted to reproduce the electrostatic potential due to the solute in its immediate environment), were obtained with the aid of the ChelpG option in B3LYP/6-311G(d) calculations.[31] The geometries of the bimolecular ion-radical complexes were based on the X-ray crystal structures presented in Table 2. A smoothed solute cavity was determined as the contact surface obtained by rolling a probe solvent molecule (taken as an effective sphere with radius r_p) over the superposition surface formed by overlapping spherical solute atoms. This procedure yielded the *solvent-excluded surface*;[46] and such a "tailor-fitted" solvent cavity,

(38) (a) Powers, M. J.; Callahan, R. W.; Salmon, D. J.; Meyer, T. J. *Inorg. Chem.* **1976**, *15*, 1457. (b) McManis, G. S.; Gochev, A.; Nielson, R. S.; Weaver, M. S. *J. Phys. Chem.* **1989**, *93*, 7733. (c) Hupp, J. S.; Dong, Y.; Blackbourn, R. L.; Lu, H. *J. Phys. Chem.* **1993**, *97*, 3278. (d) Drago, R. S.; Richardson, D. E.; George, J. E. *Inorg. Chem.* **1997**, *36*, 25. (e) Nelsen, S. F.; Trieber, D. A., II; Ismagilov, R. F.; Teki, Y. *J. Am. Chem. Soc.* **2001**, *123*, 5684.
(39) Matyushov, D. V. *J. Chem. Phys.* **2004**, *120*, 7532.
(40) It must be stressed that the calculations reported in Table 4 are based on either experimental structures and dielectric constants or the results of nonempirical (DFT) electronic structure computations, but they involve *no* parameters fitted to either kinetic or spectroscopic ET data.
(41) (a) Liu, Y.-P.; Newton, M. D. *J. Phys. Chem.* **1995**, *99*, 12382. (b) Ungar, L. W.; Newton, M. D.; Voth, G. A. *J. Phys. Chem. B* **1998**, *103*, 7367.

(42) Siriwong, K.; Voityuk, A. A.; Newton, M. D.; Roesch, N. *J. Phys. Chem. B* **2003**, *107*, 2595.
(43) See: Liu, Ungar, and Siriwong et al. in refs 41 and 42.
(44) (a) Sharp, K. A.; Nicholls, A. *Delphi*, v 3.0; 1989; See, e.g.: (b) Sharp, K. A.; Honig, B. *Ann. Rev. Biophys. Chem.* **1990**, *19*, 301. (c) *Delphi* (designed to solve the Poisson−Boltzman equation) is used here to solve the simpler Poisson equation.
(45) Sharp, K.; Arale, J. C.; Honig, B. *J. Phys. Chem.* **1992**, *96*, 3822.
(46) (a) Connolly, M. L. *Science*, **1983**, *221*, 709. (b) Richards, F. M. *Ann. Rev. Biophys. Bioeng.* **1977**, *6*, 151. (c) Tomasi, J.; Mennucci, B.; Cammi, R. *Chem. Rev.* **2005**, *105*, 2999. (d) See also: LeBard, D. N.; Lilichenko, M.; Matyushov, D. V.; Berlin, Y. A.; Ratner, M. A. *J. Phys. Chem. B* **2003**, *107*, 14509.

Chart 3. Graphical Representation of the "Tailor-Fitted" Solvation of $(TTF)_2^{+\bullet}$
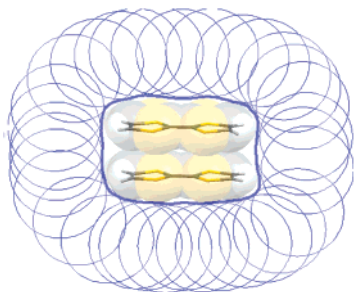
herein designated as the smoothed multisphere model (SMSM), is typically illustrated for the vertically stacked **TTF** associate in Chart 3 above.[47]

The spherical solute atom radii were taken as the van der Waals radii: 1.75 Å (C); 1.5 Å (N); 1.9 Å (S); 1.2 Å (H) in a manner similar to that employed in previous studies of molecular solutes.[48] The dielectric constants for the solvents are given in Table 3 and $\epsilon_{in} = 2$ is assigned to the solute cavity, as noted above. The values of r_p for the solvent probe molecule were taken as ~2 Å for dichloromethane and acetonitrile and as ~2.5 Å for the other five solvents.[49] The solvent reorganization energies λ_o calculated in this way for $(TTF)_2^{+\bullet}$ and $(TCNE)_2^{-\bullet}$ associates are listed in Table 4,[40,50] columns 4 and 5, respectively.

3. Discursive Summaries

The rapid bimolecular rates of electron-transfer self-exchange (fast on the ESR time scale) occur between organic electron donors (D) and their associated cation radicals, as well as electron acceptors (A) and their anion radicals, according to eqs 2 and 3, respectively; and these point to the diffusive participation of strongly coupled (1:1) precursor complexes which are spectrally observed and quantitatively characterized via their diagnostic intervalence transitions (Mulliken–Hush).

3.1. Bimolecular Ion-Radical Associates as Robin–Day (Intermolecular) Class II and Class III Precursor Complexes. The spectral (NIR) detection in Table 1 and the separate X-ray crystallographic analysis in Table 2 identify the precursor complexes: $[D,D^{+\bullet}]$ and $[A^{-\bullet},A]$ as rather loosely bonded π-associates with the relatively wide interplanar separations of $r_{DA} = 3.1 \pm 0.3$ Å, irrespective of their charge. Most importantly, the detailed spectral and X-ray analyses reveal these ion-radical associates as belonging to Robin–Day class II or class III to describe either their localized or delocalized electronic structure consisting of a double or single potential-energy minimum as qualitatively depicted above in Chart 2.

3.2. Theoretical Substantiation of Class II and Class III Precursor Complexes. Quantitative comparison of the critical electron-transfer parameter (H_{DA}) that describes the electronic

(47) Note that Chart 3 is the schematic depiction of the SMSM model used in the calculation.
(48) (a) Bondi, A. *J. Phys. Chem.* **1964**, *68*, 441. (b) Tannor, D. J.; Marten, B.; Murphy, R.; Friesner, R. A.; Sitkoff, D.; Nicholls, A.; Honig, B.; Ringnalda, M.; Goddard, W. A. *J. Am. Chem. Soc.* **1994**, *116*, 11875.
(49) (a) Matyushov, D. V.; Schmid. R. *J. Phys. Chem.* **1994**, *98*, 5152. (b) Schmid. R.; Matyushov, D. V. *J. Phys. Chem.* **1995**, *99*, 2393.
(50) Note that the values of solvent reorganization energy calculated in dichloromethane for $(TTF)_2^{+\bullet}$ complex with "slipped" geometry is 3.39×10^3 cm^{-1}; and in the "crossed" geometry, it is: 3.28×10^3 cm^{-1}.
(51) Reichardt, C. *Solvents and Solvent Effects in Organic Chemisty*; VCH: Weinheim, 1988.

Table 4. Theoretical Solvent Reorganization Energies (in 10^3 cm^{-1}) Based on the Smoothed Multisphere Model (SMSM)[46]

			$(TTF)_2^{+\bullet}$	$(TCNE)_2^{-\bullet}$
solvent	ϵ_o[a]	ϵ_∞[b]	λ_o	λ_o
CHCl$_3$	4.81	2.091	2.06	–
THF	7.58	1.98	2.99	3.54
CH$_2$Cl$_2$	8.93	2.028	3.15	3.74
acetone	20.56	1.846	4.16	4.91
DMF	36.7	2.05	4.12	4.84
CH$_3$CN	35.94	1.81	4.52	5.35
PC	64.9	2.02	4.32	5.07

[a] Static dielectric constants from ref 51. [b] Optical dielectric constants from ref 51.

Table 5. Quantitative Comparison of the Calculated Intrinsic Barrier with the Experimental Reorganization Energy Obtained from the Intervalence Absorption

	TTF			TCNE		
solvent	$\lambda_T(calc)$[a]	$\lambda_T(exp)$[b]	dev, %	$\lambda_T(calc)$[a]	$\lambda_T(exp)$[b]	dev, %
CHCl$_3$	4.36	4.65	−6	–	–	–
THF	5.29	5.13	3	5.81	6.67	−13
CH$_2$Cl$_2$	5.45	4.73	15	6.01	6.6	−9
acetone	6.46	5.71	13	7.18	7.35	−2
DMF	6.42	5.92	8	7.11	7.41	−4
CH$_3$CN	6.82	5.81	17	7.62	7.25	5
PC[a]	6.62	5.71	16	7.34	7.37	0

[a] $\lambda_T(calc) = \lambda_o(calc) + \lambda_{in}(calc)$ (where $\lambda_{in} = 2300$ and 2270 cm^{-1} for $(TTF)_2^{+\bullet}$ and $(TCNE)_2^{-\bullet}$) obtained from DFT calculations.[7,8a] [b] Based on $\lambda_T(exp) = \nu_{IV}$.

coupling or binding energy within the bimolecular precursor complex as obtained by ab initio and DFT computations of the X-ray structures of the ion-radical associates, accord with the experimental energies evaluated from the intervalence transitions. Thus, the structure-by-structure comparisons in Table 3 establish the exceptional coincidences of the experimental and theoretical values of H_{DA} for the strongly coupled class III associates: $(OMA)_2^{+\bullet}$, $(OMB)_2^{+\bullet}$ and $(NAP)_2^{+\bullet}$. Moreover, equally good agreements are also observed with $(DDQ)_2^{-\bullet}$, $(DBQ)_2^{-\bullet}$ and $(TCNQ)_2^{-\bullet}$ that lie at or close to the class II/III border. However, it is notable in Table 3 that the experimental values of H_{DA} for the more weakly coupled class II complexes: $(TTF)_2^{+\bullet}$ and $(TCNE)_2^{-\bullet}$ both deviate from the calculated values. Indeed, such an enhanced discrepancy is related to the lower (thermodynamic) stability of $(TTF)_2^{+\bullet}$ and $(TCNE)_2^{-\bullet}$ relative to the $(OMB)_2^{+\bullet}$ and $(OMA)_2^{+\bullet}$ as measured by their values of K_{DA} in Table 1. As such, these ion-radical associates are expectedly more labile in solution; and the (averaged) interplanar separation parameter r_{DA} used in the experimental evaluation of H_{DA} may be underestimated relative to that measured in the X-ray structure.[37] With these accountable exceptions, the theoretical results in Table 4 thus clearly identify the direct relevance of the solid-state structures of the ion-radical associates to class II and class III precursor complexes that are spectrally characterized in solution.

3.3. Quantitative Evaluation of Solvent Perturbations of the Intervalence Transitions in Bimolecular Precursor Complexes. The experimental observation of the solvent effect imposed on the bimolecular precursor complex resides, according to Marcus theory, in the evaluation of the intrinsic reorganization barrier $(\lambda_T = \lambda_o + \lambda_i)$, which is directly related to the intervalence transition in the case of class II complexes.

Theoretical values of the inner-sphere reorganization energies of the class II complexes: $(TTF)^{+\bullet}$ and $(TCNE)_2^{-\bullet}$ were pre-

viously evaluated as: $\lambda_i = 2300$ and 2270 cm^{-1}, respectively,[7,8a] and these coupled with the values of the solvent reorganization energy (λ_o) in Table 4 lead to the calculated intrinsic barrier (λ_T) in Table 5 that are in rather good agreement with those based on experimental intervalence transitions (columns 3 and 6).[52b] Such an intimate concord of experiment and theory thus provides unambiguous validation of the X-ray structures (Table 2) as the relevant precursor complex in bimolecular electron transfer as modulated by solvent variation.[52]

4. Conclusion

The unambiguous identification and quantitative characterization of the critical precursor complex in the bimolecular electron-transfer mechanism for ion-radical exchanges (eqs 2 and 3) are accomplished for the first time by rigorously establishing the *direct* tie-in of the transient species (adumbrated in solution) with the crystalline associate (elucidated by X-ray crystallography). Since the latter is an ambiguity common to many mechanistic problems,[53] it was our intent to demonstrate how the invocation of theoretical constructs, in this case Marcus—Hush electron-transfer theory, can bridge the intrinsic (solution/solid-state) disconnect via the application of quantitative solvent probes.

Thus, the distinctive modulation of the diagnostic intervalence absorption bands by various solvents, as clearly delineated in Figures 2 and 3, identifies the existence of two basic types of ion-radical precursor complexes that belong to either Robin—Day class II (localized) or class III (delocalized),[54] the transition energies of which *are* or *are not* solvent dependent. As such, the theoretical calculations of the electronic coupling elements (H_{DA}) and the reorganization energies (λ_T) provide the requisite probe for class II and class III behaviors that are the distinguishing characteristics of bimolecular precursor complexes as provided by combined spectral/X-ray analyses.

5. Experimental Methods

Materials. Octamethylbiphenylene (**OMB**), octamethylanthracene (**OMA**), and dibromodicyano-*p*-benzoquinone (**DBQ**) were synthesized according to the reported procedures.[8,55] Tetrathiafulvalene (**TTF**), dichlorodicyano-*p*-benzoquinone (**DDQ**), and tetracyanoethylene (**TCNE**)

from commercial sources were repurified by sublimation in vacuo and/or recrystallization. The ion-radical salts with either the bulky non-coordinating counterion, *closo*-dodecamethylcarboranate (CB$^-$), or ligated alkali-metal cations encapsulated within the cavity of a [2,2,2]-cryptand or sandwiched between a pair of appropriate crown-ethers [M$^+$(L)] were prepared as described previously.[8] Acetonitrile, acetone, chloroform, dichloromethane, diethyl ether, propylene carbonate, tetrahydrofuran, dimethylformamide, and hexane were purified according to standard laboratory procedures[56] and were stored in Schlenk flasks under an argon atmosphere prior to use.

Electronic absorption spectra were recorded on a Varian Cary 5 (200−3000 nm) spectrometer in Teflon-capped quartz cuvettes under an argon atmosphere. Formation of the ion-radical associates: (D)$_2^{+\cdot}$ and (A)$_2^{-\cdot}$ complexes was also studied under an argon atmosphere at room temperature (22 °C) in various solvents similar to the procedure in dichloromethane described earlier.[8] The measurement of the newly formed NIR bands (in the 1000−3000 nm range) was carried out by addition of the donor to the solution of its cation radical, or the acceptor was added to the solution of its anion radical. The quantitative analysis of the NIR intensities was carried out as described earlier.[8]

Crystallographic data for the X-ray studies were collected at −100 °C with a Bruker SMART Apex diffractometer equipped with a CCD detector using Mo Kα radiation ($\lambda = 0.71073$ Å), and the structures were solved by direct methods and refined by full matrix least-squares procedure.[57] The crystallographic data and the details of the structure refinements for **DBQ**, Na(12crown4)$_2^+$(**DBQ**)$^{-\cdot}$, and Na(12crown4)$_2^+$(**DBQ**)$_2^{-\cdot}$ are presented in Table S1 in Supporting information.

The details of the ab initio computations of the electronic coupling elements and reorganization energy were presented previously[7,8] (see also Supporting Information for details).

Supporting Information Available: The crystallographic data and the details of the structure refinements for **DBQ**, Na(12crown4)$_2^+$(**DBQ**)$^{-\cdot}$ and Na(12crown4)$_2^+$(**DBQ**)$_2^{-\cdot}$ (Table S1), details of the electronic coupling elements computations (Table S2), details of reorganization energy computations (Tables S3), complete ref 31, orthogonal coordinates of the ion-radical associates employed in the calculations of coupling elements and solvent reorganization energies and ESP charges employed in the calculations of the solvent reorganization energies. This material is available free of charge via the Internet at http://pubs.acs.org.

JA076591B

(52) (a) Note that the values of reorganization energies (λ_T) calculated as the sum of inner-sphere and outer-sphere components are (in 10^3 cm^{-1}): 4.9 for (**OMB**)$_2^{+\cdot}$, 3.4 for (**OMA**)$_2^{+\cdot}$, 4.9 for (**NAP**)$_2^{+\cdot}$, 6.4 for (**DDQ**)$_2^{-\cdot}$, and 4.9 for (**TCNQ**)$_2^{-\cdot}$ in dichloromethane (see Table S2 in Supporting information for calculation details). The comparison of these values with the electronic coupling elements in Table 3 supports our assignment of (**OMB**)$_2^{+\cdot}$, (**OMA**)$_2^{+\cdot}$, and (**NAP**)$_2^{+\cdot}$ as Robin−Day class III complexes because $\lambda_T < \nu_{iv}$. Likewise, (**DDQ**)$_2^{-\cdot}$ and (**TCNQ**)$_2^{-\cdot}$ are borderline class II/III complexes because $\lambda_T \approx \nu_{iv}$. (b) We anticipate that more quantitative *molecular* models of solvation[39] would help to further quantify class II, class III, and especially the borderline class II/III behaviors, and in addition, to provide deeper insight into the solvent effect on the intervalence transition of class II complexes.

(53) In a more general context, it is amusing to note that the extensive usage of a similar structural disconnect between complex mechanistic pathways (in solution) versus the isolation and X-ray analysis of the crystalline state commonly pervades the biochemical literature, especially those relating to enzyme/substrate recognitions. Compare e.g.: Wigley, D. B. *Ann. Rev. Biophys. Biomol. Struct.* **1995**, *24*, 185.

(54) For the distinctive kinetics behavior of bimolecular ET reactions proceeding via class III precursor complexes, see Sun et al. in ref 28.

(55) (a) Wallenfels, K.; Bachman, G.; Hofmann, K.; Kern, R. *Tetrahedron* **1965**, *21*, 2239. (b) Rathore, R.; Bosch, E.; Kochi, J. K. *Tetrahedron Lett.* **1994**, *35*, 1335.

(56) Perrin, D. D.; Armagero, W. L.; Perrin, D. R. *Purification of Laboratory Chemicals*, 2nd ed; Pergamon: New York, 1980.

(57) (a) Sheldrick, G. M. *SADABS*, Ver. 2.03; Bruker/Siemens Area Detector Absorption and Other Corrections, 2000. (b) Sheldrick, G. M. *SHELXS 97*: Program for Crystal Structure Solutions; University of Göttingen: Germany, 1997. (c) Sheldrick, G. M. *SHELXL 97*: Program for Crystal Structure Refinement; University of Göttingen: Germany, 1997.